Civil and Environmental Engineering
Vol. 0, Issue 0, DOI: 10.2478/cee-2026-0083

Land Use and Land Cover and Their Impacts on Land Surface Temperature in the Little Zab River Basin: A Predictive Study

Nadheer AYOOB[1,2,*], Ruqayah MOHAMMED[1]

[1] Civil Engineering Department, Faculty of Engineering, The University of Babylon, Hilla, Iraq.

[2] Civil Engineering Department, College of Engineering, Wasit University, Wasit, Iraq.

* Corresponding author: nadheer.ayoob.engh360@student.uobabylon.edu.iq

Date of Submission: 01 December 2025
Revision Date: 02 January 2026
Date of Acceptance: 05 January 2026

Civil and Environmental Engineering
Journal of the Faculty of Civil Engineering | University of Žilina

Abstract

During the past century, the Little Zab River Basin (LZRB) experienced obvious Land Use and Land Cover Alterations (LULCA) due to human-induced and natural causes. LULC has a great impact on the basin's hydrological characteristics, including evapotranspiration, surface runoff, and Land Surface Temperature. The current research investigated LULCA in the LZRB throughout two decades (from 2002 to 2023), and projected future trends for 2050. Additionally, this study used a Multiple Linear Regression (MLR) model to predict Land Surface Temperature (LST) for 2050. Highly classified maps are produced using the Maximum Likelihood Algorithms (MLA), with Kappa indices ranging from 0.90 to 0.94. The analysis of the past period showed significant LULCA across the basin. Between 2002 and 2023, the watershed experienced a considerable growth in urban areas, reaching 168.09%, while agricultural lands increased by 42.13%. Moreover, the Normalized Difference Vegetation Index (NDVI) increased from 0.16 in 2002 to 0.24 in 2023. The LST declined by 6.67% during the same period. The projected results for 2050, derived using the CA-Markov model, with a Kappa standard index of 0.77, and a calibrated MLR model, with very good to satisfactory statistical results, revealed similar trends. The predicted LULC map showed an additional increase in agricultural lands and urban areas. Finally, the NDVI value exhibited a 37.50% rise, and the LST is projected to decline by 7.67% in 2050 compared to the 2023 value.

Keywords

Little Zab River Basin; Land Use and Land Cover; Land Surface Temperature; NDVI.

1. Introduction

The sustainable management of water resources and environmental systems in watersheds has garnered heightened attention both locally and worldwide due to its significance for ecosystem preservation (Idrees, M. et al., 2022; Voon, K.L. et al., 2022; Masdaf, N. et al., 2025). Land use and land cover (LULC) have a significant influence on long-term ecological sustainability (Jafarzadeh, F. et al., 2018; Costa, R.C.A. et al., 2023). Land use and land cover alteration (LULCA) has emerged as a global interest, generating heightened concern among managers and policymakers about its potential impact on water resources, the environment, and watershed hydrology (Mahdi, Z. and Mohammed, R., 2022b; Özturk, B. et al., 2023). The identification of historical and prospective alterations in LULC has become an essential component in tracking and evaluating biodiversity, air pollution, and hydrology to reduce anthropogenic impacts on the environment

(Jafarzadeh, F. et al., 2018; Amgoth, A. et al., 2023). LULCA induces both short-term and long-term alterations in a watershed, influencing its surface runoff, groundwater recharge, evapotranspiration, and flood peaks (Gashaw, T. et al., 2018; Teshome, D. et al., 2023).

Furthermore, LULC dynamics have a considerable influence on Land Surface Temperature (LST). The LST refers to the radiating-layer temperature of the ground's surface, which directly regulates the air temperature of the next atmospheric layer and serves as an indicator of surface energy, impacting the world environment. The acquisition of LST is advantageous in several research fields related to climate change, vegetation monitoring, and the hydrological cycle (Faqe, G., 2017). In addition to LULC, variables influencing LST include topographical conditions and urban growth (Khan, M. et al., 2022).

Latest advancements in remote sensing methodologies and geographical information systems have exhibited significant efficacy in analyzing historical and projected LULC patterns and their associated LST (Sathe, T. and Rahman, S., 2023; Abdulsahib, S. et al., 2024; Ayoob, N. and Mohammed, R., 2025). The image classification process is categorized into two primary types: unsupervised and supervised methods. Unsupervised methods are applicable in the absence of ground reference data (Abburu, S. and Golla, S.B., 2015). On the other hand, supervised techniques provide the capability for mistake identification and correction, which are their fundamental advantages (Nath, S. et al., 2014). Numerous classification techniques exist, with the maximum likelihood algorithm (MLA) the most prevalent supervised method according to its accuracy across different study areas (Chughtai, A. et al., 2021).

Several models have recently been developed to forecast future LULC based on historical LULC patterns (Khan, M. et al., 2022). The prediction algorithms include cellular automata (CA), artificial neural networks (ANN), and Markov chains (Fetene, T. et al., 2023). The combination of two algorithms has been applied to provide improved outcomes (Atef, I. et al., 2023). Thus, many integrated CA approaches have been developed, including CA-ANN (Ullah, S. et al., 2019; Fetene, T. et al., 2023), CA-Markov (Al-sharif, A. and Pradhan, B., 2014; Manakane, S. et al., 2023), and WoE-CA (Khan, M. et al., 2022).

Spectral indices have been employed to project LST (Khan, M. et al., 2022). Ullah, S. et al. (2019) utilized NDBaI, NDBI, and UI, while Kafy, A. et al. (2021) used NDVI, NDBI, and NDWI to predict LST. Al-Doski, J. et al. (2013); Khan, M. et al. (2022) relied on NDVI to model LST, asserting that NDVI has a high adverse relationship with LST. On the other hand, Mansourmoghaddam, M. et al. (2023) directly predicted LST using a Markov model.

The Middle East is considered one of the areas most susceptible to the effects of climate change, such as desertification, owing to raised LST and reduced precipitation (Pathak, M. et al., 2022; Abdulsahib, S. et al., 2024). Iraq is one of the Middle Eastern countries that has seen substantial LULCA due to climate change, population expansion, and a succession of conflicts. Consequently, several studies of past and projected LULC patterns are essential for improving future planning intended at accomplishing environmental conservation (Mahdi, Z. and Mohammed, R., 2022a). Numerous research works have been conducted in Iraq on the fields of LULC and LST, including those by Gaznayee, A. et al. (2022); Hashim, M. et al. (2022); Al-Taei, A. et al. (2023); Rash, A. et al. (2023). Nonetheless, a limited number of studies have addressed the issue at a basin scale. Younus, M. and Mohammed, R. (2023) utilized the MLA to analyze LULCA in the Diyala River Watershed between 2013 and 2022, and determined the corresponding LST during the same timeframe.

The Little Zab River Basin (LZRB) is an important area for agriculture, biodiversity, and natural resources, as well as for supplying the Tigris River with water (Mohammed, R. and Scholz, M., 2024). Previous studies have been conducted in the basin to investigate the effects of climate change (Abbas, N. et al., 2016), groundwater recharge (Rahem, M. and Mohammed, R., 2025), and historical and projected LULCA (Mahdi, Z. and Mohammed, R., 2022b, 2022a). Nevertheless, a comprehensive study to examine the relationship between past LULC and LST and to assess the future LST has been lacking.

The current investigation is conducted to fill the aforementioned knowledge gap. Accordingly, this study involved three primary objectives: (1) to determine the historical LULC dynamics in the LZRB and their impacts on both NDVI and LST, (2) to project LULC and NDVI in 2050 by the widely-used CA-Markov model for evaluating future tendencies, and (3) to formulate a novel multiple linear regression model predicting LST in 2050. Generally, this study's findings provide policymakers with crucial data to formulate sustainable strategies to conserve the LZRB's resources and environment.

2. Methodology

The methodology followed in this study is displayed in Figure 1.

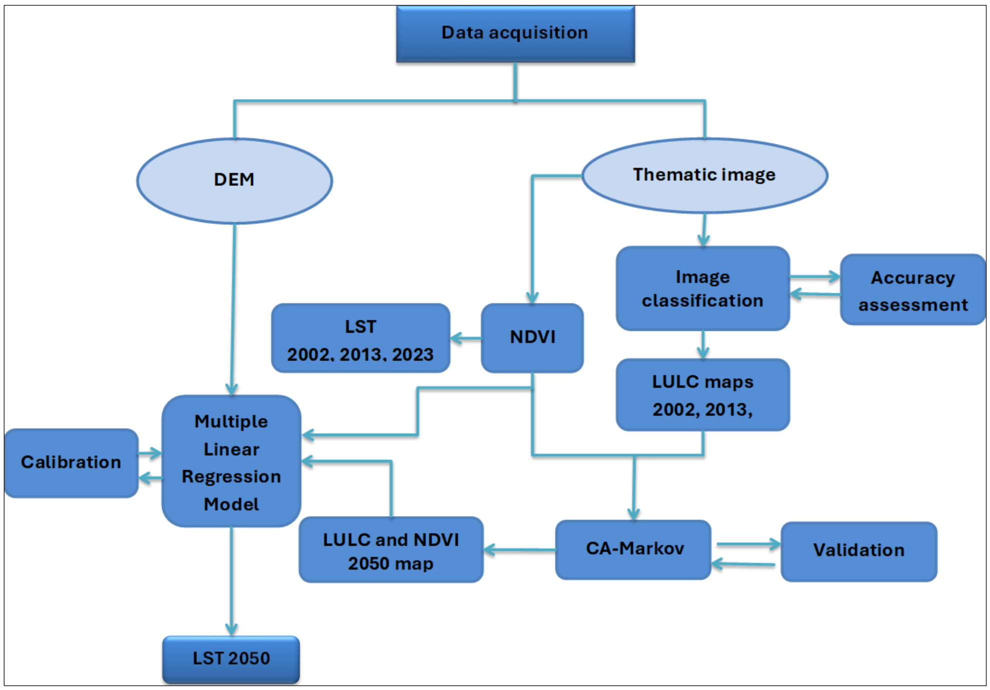

Figure 1: Flowchart of the research

2.1. Study Area

The Little Zab River Basin is a common catchment area located in northwestern Iran and northeastern Iraq, as shown in Figure 2. The basin covers an area of about 19800 km^2, with approximately 76% located within Iraq, while the rest is situated in Iran (Mahdi, Z. and Mohammed, R., 2022b, 2022a).

The topography gradually varies from level grounds in the southwestern parts to hills and mountains in the northeastern parts (Al-Saady, Y. et al., 2022). The basin's climate is characterized as semi-arid to arid, featuring dry and hot summers, contrasted with cold and rainy winters (Abbas, N. et al., 2016; Al-Saady, Y. et al., 2022). The average air temperature varied from 24.5 °C in the south to 9 °C in the north (Al-Saady, Y. et al., 2016; Al-Saady, Y. et al., 2022).

The Little Zab River drains the watershed. It is a 6th-order river with a total length of 372 km. Precipitation and ice melting fed the river. Thus, the stream flow is high in spring and reduces during summer (Al-Saady, Y. et al., 2022; Mahdi, Z. and Mohammed, R., 2022b).

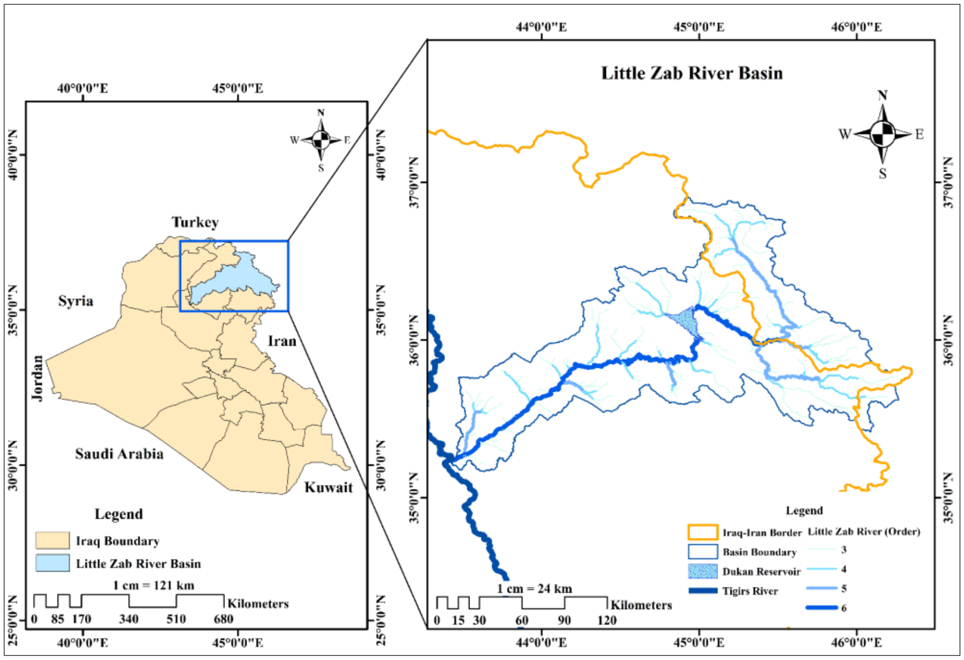

Figure 2: Details of the study area

2.2. Digital Elevation Model

The current investigation utilized a Digital Elevation Model (DEM) downloaded free of charge from the United States Geological Survey (USGS). A total of 9 DEM images with a resolution of 30 m were mosaicked to delineate the boundaries of the basin. Figure 3 displays the extracted digital elevation model of the LZRB. As shown in the figure, the majority of the basin is represented by the elevation class 500–1500 m (49.35%), followed by the classes 120–500 m (27.46%) and 1500–2500 m (21.61%), while class 2500–3599 m covers only 1.57% of the basin.

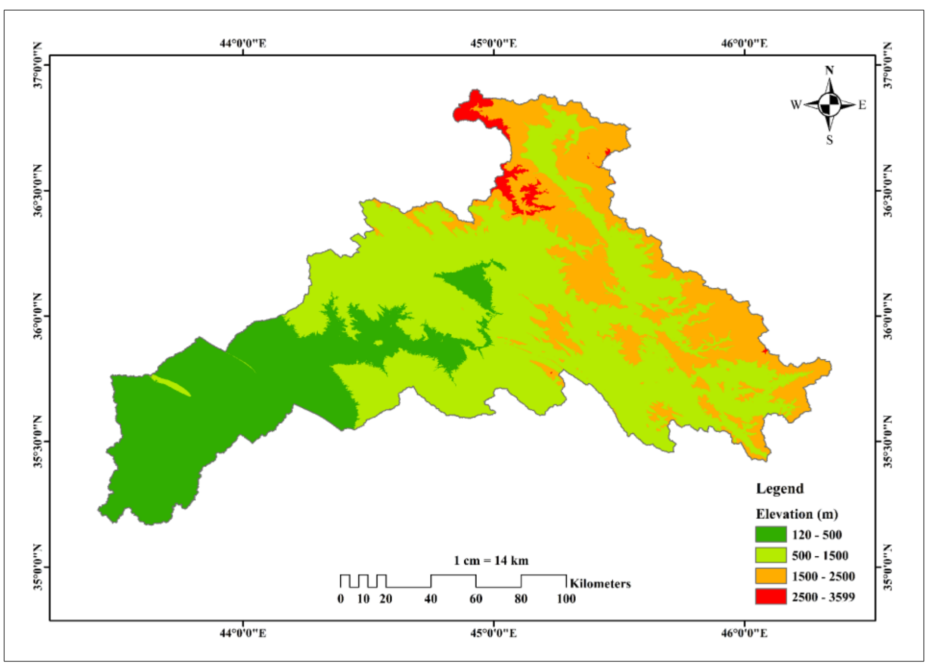

Figure 3: The digital elevation model of the Little Zab River Basin

2.3. Satellite Images

Landsat 5 TM, 8 OLI, and 9 OLI were used to gather satellite images for 2002, 2013, and 2023, respectively. A total of 4 tiles were mosaicked to retrieve the LULC, NDVI, and LST for the LZRB over three study years. More details about the satellite images are mentioned in Table 1. All the remotely sensed images were acquired during a month to reduce the consequences of seasonal change (Khan, M. et al., 2022). The satellite images were downloaded with cloud cover below 2% to enhance the classification precision. Daytime imageries were utilized because LST is related to solar action (Sathe, T. and Rahman, S., 2023).

Table 1: Details of the downloaded satellite images for the Little Zab River Basin

Data	Year	Acquisition Date	Satellite	Sensor	Cloud cover [%]	Resolution [m]
Satellite Imagery	2002	03 July 12 July	Landsat 5	TM[a]	0	30
	2013	02 August 26 July	Landsat 8	OLI/TIRS[b]	0.02	30/15[c]
	2023	05 July 17 July	Landsat 9		0.77	

Path/row = 168-169/34-36;

Coordinate system: WGS 1984/ UTM Zone 38N

Source: USGS ((https: //earthexplorer.usgs.gov/)

[a] Thematic Mapper.

[b] Operational Land Imager and Thermal Infrared Sensor.

[c] The 8th band is utilized to enhance the 30-meter resolution to 15 m.

The LULC maps for the three years (2002, 2013, and 2023) were retrieved from the pre-processed Landsat images by ERDAS IMAGINE 2014. According to a comprehensive investigation of the study area and based on previous studies by Gaznayee, A. et al. (2022); Mahdi, Z. and Mohammed, R. (2022a), the LZRB were classified into bare lands, forests, agricultural lands, urban areas, and water bodies (Table 2).

Table 2: Description of land use and land cover classes

Class	Description
Bare lands (BL)	Lands lack obvious vegetation cover, including burnt agricultural lands.
Forests (F)	Shrub lands, and artificial and natural trees.
Agricultural lands (A)	Lands showed apparent greenness, including crop grounds.
Urban areas (UA)	Transportation networks, settlements, and industrial regions.
Water bodies (WB)	Lands covered with water, including reservoirs, artificial and natural streams, and fishponds.

The image classification process in this study was performed using the maximum likelihood algorithm (MLA). The MLA represents a very strong and common supervised classification method (Srivastava, P. et al., 2012; Khan, M. et al., 2022). It relied on a group of training samples specified by a user for each LULC class (Ahmed, B. et al., 2013; Khan, M. et al., 2022).

The process of accuracy evaluation was performed employing the stratified random method to check the compatibility between real and classified maps by comparing the classification outcomes with reference data (Kafy, A. et al., 2021; Mahdi, Z. and Mohammed, R., 2022a; Fetene, T. et al., 2023; Younus, M. and Mohammed, R., 2023). Three hundred points were investigated for each map, with fifty points per LULC class. The required statistical indices were determined by preparing the error matrix. The indices comprised overall accuracy, producer's and user's accuracies, as well as the Kappa index (KI). The KI is a method employed for comparing LULC maps (Zadbagher, E. et al., 2018; Khan, M. et al., 2022).

2.4. Normalized Difference Vegetation Index

The NDVI was commonly employed to assess the state of vegetation cover. So, NDVI serves as a reliable measure for assessing drought conditions. The following formula was employed to determine the NDVI value:

$$\mathrm{NDVI} = \frac{\mathrm{NI} - \mathrm{R}}{\mathrm{NI} + \mathrm{R}} \tag{1}$$

Where:

NI - near-infrared band,

R – red band.

Table 3 categorizes vegetation density based on the NDVI (Alex, E. et al., 2017; Gaznayee, A. et al., 2022). The ENVI software offers a simple function for calculating NDVI.

Table 3: Explanation of the Normalized Difference Vegetation Index (NDVI) classes

Feature	NDVI range
Water, cloud, and snow	NDVI ≤ 0
Urban areas and/or bare lands	0 < NDVI ≤ 0.2
Sparse vegetation	0.2 < NDVI ≤ 0.6
Dense vegetation	0.6 < NDVI ≤ 1

2.5. Land Surface Temperature

The LST has been derived from the Landsat images' thermal bands for the years 2002, 2013, and 2023. The thermal bands for both Landsat 8 and 9 are bands 10 and 11, while the 6^{th} band is the thermal band for Landsat 5. The following methodology was applied to determine LST (Das, N. et al., 2021; Mansourmoghaddam, M. et al., 2023):

1. Calculation of the emissivity (ε):

The following formula was used to calculate the vegetation proportion (Pv) based on the NDVI values:

$$\mathrm{P_v} = \left[\frac{\mathrm{NDVI} - \mathrm{NDVI_{Lowest}}}{\mathrm{NDVI_{Highest}} - \mathrm{NDVI_{Lowest}}}\right]^2 \tag{2}$$

Where:

$NDVI_{Lowest}$ - lowest NDVI value,

$NDVI_{Highest}$ - highest NDVI value.

After that, Eq. 3 was used to calculate the land surface emissivity (ϵ) (Das, N. et al., 2021; Mansourmoghaddam, M. et al., 2023):

$$\epsilon = 0.004 \times \mathrm{P_v} + 0.986 \tag{3}$$

2. The brightness temperature:

The radiometric calibration was carried out for the Landsat images' thermal bands. Then, the emitted radiance (λ) was calculated by directing the radiance calibration. Finally, brightness temperature (BT) is calculated as follows:

$$\mathrm{BT} = \frac{\mathrm{K_2}}{\ln\left(\left(\frac{\mathrm{K_1}}{\lambda}\right) + 1\right)} \tag{4}$$

Where:

BT - brightness temperature,

K_1 and K_2 - thermal coefficients in the metadata file of the Landsat image,

λ - emitted radiance.

The ENVI program was used to determine BT. The last step included converting BT into Celsius degrees as follows (Tran, D. et al., 2017; Das, N. et al., 2021; Khan, M. et al., 2022; Sathe, T. and Rahman, S., 2023):

$$\mathrm{BT}\ (°\mathrm{C}) = \mathrm{BT} - 273.15 \tag{5}$$

3. LST retrieval:

The land surface temperature (°C) was calculated as follows (Tran, D. et al., 2017; Das, N. et al., 2021; Khan, M. et al., 2022; Sathe, T. and Rahman, S., 2023):

$$\mathrm{LST} = \frac{\mathrm{BT}}{\left(1 + (\lambda \times \frac{\mathrm{BT}}{\rho} \times \ln \epsilon)\right)} \tag{6}$$

Where:
ρ - a factor determined using Planck's constant, Boltzmann's constant, and the velocity of light.

2.6. Prediction of future LULC and LST maps

The CA-Markov chain model in IDRISI Selva software was used in this study to project a LULC map for the year 2050. Two LULC maps (2002 and 2013) were used to calculate the transition probability matrix using the Markov model. After that, the CA-Markov model was used to project the future LULC (2023). Several trials were conducted to find the optimum number of iterations. The iterations used were 1 to 10, 15, 25, 35, and 50. There are three statistical indices used to evaluate the projection accuracy: they are Kappa Standard (Kst), Kappa No Information (Kno), and Kappa Location (Kloc). The first index determines the specific quality after excluding random agreement, making the measure more stringent and accurate for spatial quality. In contrast, the Kno index evaluates the accuracy of a prediction model with no information (i.e., random prediction). Finally, the Kloc index measures the accuracy of the location of each class (Al-sharif, A. and Pradhan, B., 2014; Gaznayee, A. et al., 2022).

To calculate the future LST in the basin for 2050, a multiple linear regression model was prepared (Faqe, G., 2017). The factors included in the model were the LULC class, DEM, year, and NDVI. The regression model was obtained using SPSS software, based on 72 points from 2002 and 2013 maps. Sampling processes were carried out in ArcMap software by displaying DEM, NDVI, and LULC maps for a specific year and selecting a random pixel. The value of its elevation and NDVI, and the type of LULC were recorded for this pixel. The LULC type was recorded in 0 and 1 form. For example, if the LULC type for a given pixel is forest, it is recorded as 1 for the forests and 0 for the remaining LULC classes. The merit of using 0 and 1 values for the LULC classes is that they convert the descriptive data to numerical form, which the model can understand without imposing an incorrect mathematical order among the classes, thereby offering high precision to estimate the isolated effect of each LULC class on LST. After formulating the equation, 36 reference points were selected from the 2023 LST maps to validate the generated LST formula. The LULC and NDVI maps in 2050 are required to create the 2050 LST map. The NDVI maps of 2002 and 2013 were used to project the 2023 map using the CA-Markov model, which was evaluated for its efficiency before projecting the 2050 NDVI map.

3. Results and Discussion

3.1. Past LULC Dynamics

The statistical measures used to assess the accuracy of image classification are listed in Table 4. The highest and the lowest overall accuracy were 91.70% (2013) and 94.70% (2023), respectively. Values of the Kappa index obtained were 0.91, 0.90, and 0.94 for 2002, 2013, and 2023, respectively. Therefore, the classified maps were almost perfect, since the

Kappa index exceeded 0.81 (Congalton, R., 2001; Rwanga, S. and Ndambuki, J., 2017). However, urban areas exhibited the lowest user's accuracy, ranging from 76% to 88%. This can be attributed to the spectral similarity between the asphalt and concrete surfaces and the bare lands in the LZRB. This spectral overlap led to the misclassification of bare lands as urban areas (i.e., commission error) (Du, P. et al., 2014; Ayoob, N. and Mohammed, R., 2025).

Table 4: Results of the accuracy assessment process

LULC class	2002		2013		2023	
	U[a]	P[b]	U	P	U	P
Agricultural lands	98.00	92.45	90.00	93.75	92.00	92.00
Bare lands	98.00	85.74	99.00	85.29	99.00	93.10
Forests	88.00	97.78	88.00	91.67	90.00	93.75
Urban areas	76.00	100.00	76.00	100.00	88.00	100.00
Water bodies	98.00	100.00	98.00	100.00	100.00	98.04
Overall accuracy [%]	92.67		91.67		94.67	
Kappa index	0.91		0.90		0.94	

Notes: [a] user's accuracy, [b] producer's accuracy.

Figures 4 and 5 show that bare lands covered the main portion of the LZRB. The coverage ratio of the bare lands was 58.95 in 2002. This percentage reduced to 56.04% and 54.10% in 2013 and 2023, respectively. Forests covered 37.05%, 38.97%, and 39.72% of the catchment area in 2002, 2013, and 2023, respectively. Urban areas covered 186.38, 325.79, and 498.29 km^2 in 2002, 2013, and 2023, respectively, with a total expansion of 311.91 km^2. Thus, the urban area expanded significantly by 75.53% and 168.09% in 2013 and 2023, respectively, as compared to the area in 2002. The total area of water bodies was 257.27 km^2 in 2002, reduced to 200.95 km^2 in 2013, and then increased to 222.64 km^2, resulting in a total decline of 13.49% from 2002 to 2023.

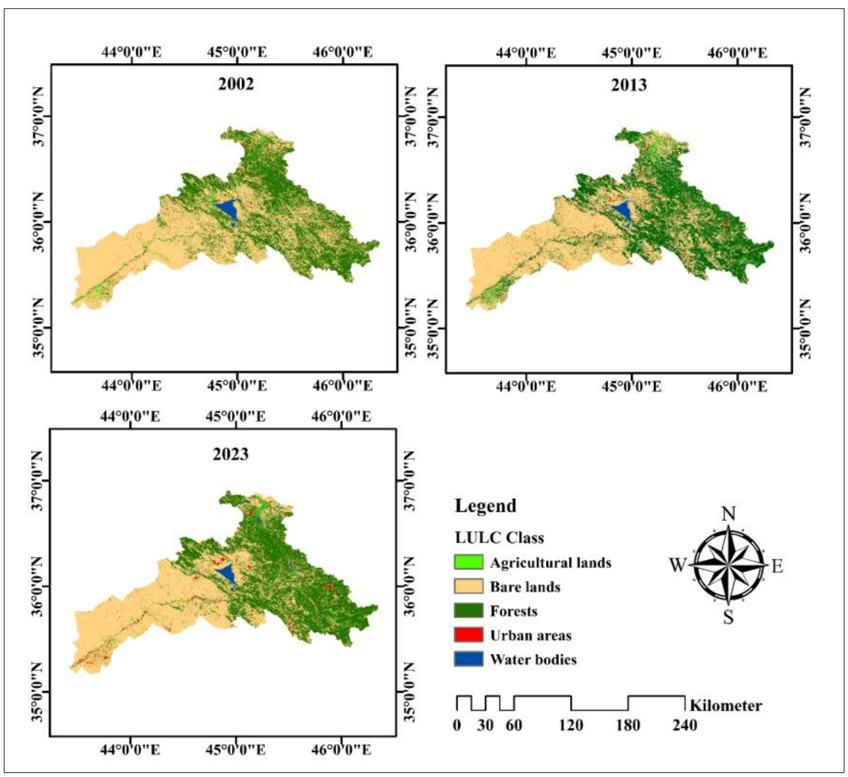

Figure 4: Distribution of LULC within the LZRB

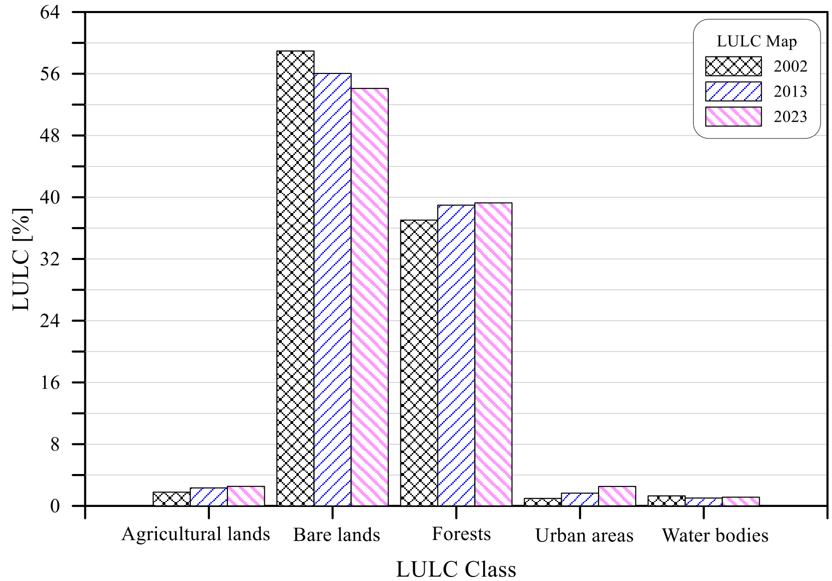

Figure 5: Coverage ratio of LULC in the LZRB

3.2. Variation in The Past NDVI

The spatial distribution of NDVI classes throughout the investigation period is presented in Table 5 and Figure 6. The class 0–0.2 (no vegetation) decreased from 73.30% in 2002 to 59.50% in 2013 and 46.50% in 2023. In contrast, the 0.6–1 class (dense vegetation) increased by 250% and 500% in 2013 and 2023, respectively, compared with 2002. Furthermore, the mean NDVI value was 0.16, 0.20, and 0.24 in 2002, 2013, and 2023, respectively.

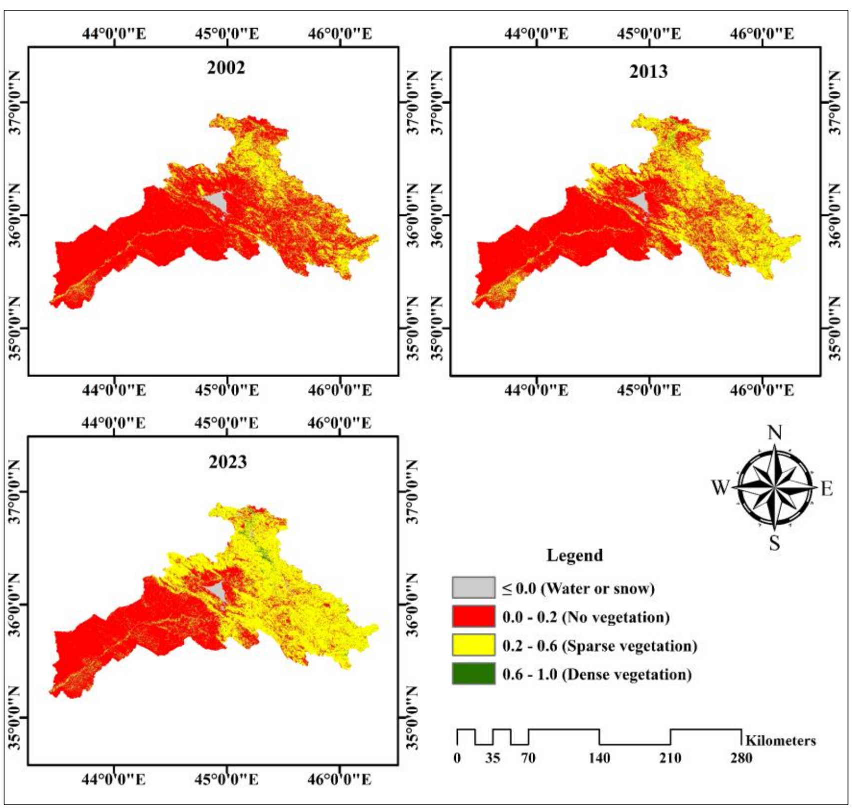

Figure 6: Distribution of NDVI classes within the LZRB

Table 5: Areas of the NDVI classes in the study area

Year	2002		2013		2023	
Class	Area					
	[km²]	[%]	[km²]	[%]	[km²]	[%]
≤ 0	251.5	1.3	196.5	1.0	220.1	1.1
0 – 0.2	14501.9	73.3	11783.3	59.5	9201.3	46.5
0.2 – 0.6	5002.8	25.3	7679.9	38.8	10134.4	51.2
0.6 – 1	38.00	0.2	134.3	0.7	238.2	1.2

3.3. Variation in The Past LST

The LST in the Little Zab River Basin was classified into six classes, as displayed in Figure 7 and listed in Table 6. The 45−50 °C class was the most prevalent in 2002 and 2013, while in 2023, the dominant class was 40−45 °C. The ratio of class > 50 °C (i.e., the highest class) reduced by 62.64% and 82.60% in 2013 and 2023, respectively, compared to the value in 2002. The average LST within the basin was 44.24 °C in 2002, then decreased to 43.44 and 41.29 °C in 2013 and 2023, respectively. Figure 7 shows that the northern areas of the watershed had the lowest LST, whereas the western portions recorded the highest LST.

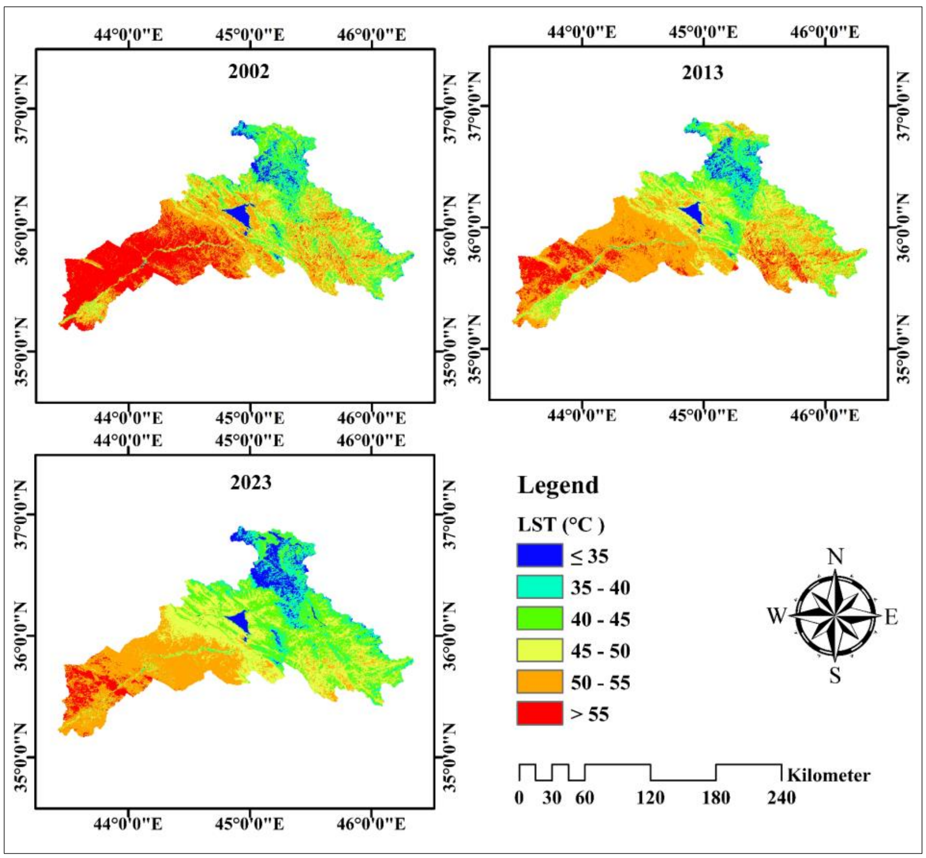

Figure 7: Distribution of LST classes within the LZRB

Table 6: Areas of the LST classes in the study area

Year	2002		2013		2023	
Class [°C]	Area					
	[km²]	[%]	[km²]	[%]	[km²]	[%]
≤ 30	664.71	3.36	566.48	2.86	1236.78	6.25
30 – 35	1617.81	8.17	1615.61	8.16	2300.63	11.62
35 – 40	3067.56	15.50	2933.72	14.82	4489.89	22.68
40 – 45	4290.98	21.68	5054.64	25.54	5495.16	27.76
45 – 50	5274.30	26.65	7800.91	39.41	5421.87	27.39
> 50	4878.62	24.65	1822.68	9.21	849.82	4.29

3.4. Future LULC Pattern

The classified LULC maps for 2002 and 2013 were used to project the 2023 map. The projected and classified LULC maps for 2023 were compared to evaluate the efficiency of the CA-Markov model. The model was run with various iterations, ranging from 1 to 50, to determine the optimum iteration value. Figure 8 shows the effect of the iteration number on the projection accuracy.

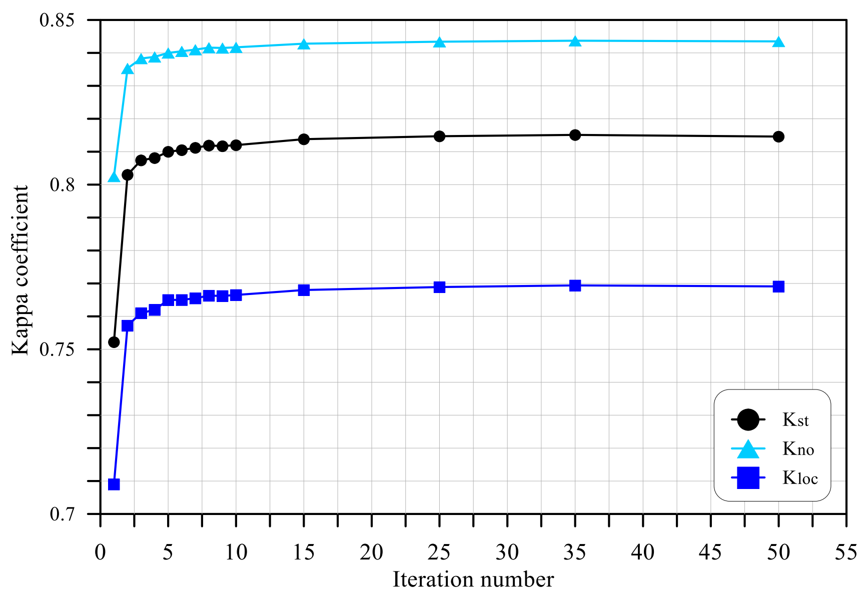

Figure 8: Iteration number versus Kappa coefficient

The figure exhibits that projection accuracy increases significantly as the iteration number increases from 1 to 15. The rate of accuracy enhancement decreases after 15 iterations, while the model efficiency exhibits a decline after 35 iterations. Accordingly, a 15-iteration run was performed in this study because it combines high accuracy with a feasible execution time. The obtained K-standard, K-no, and K-location were 0.77, 0.84, and 0.81, respectively. The Kappa coefficients indicated a good performance for the CA-Markov model (Al-sharif, A. and Pradhan, B., 2014; Mahdi, Z. and Mohammed, R., 2022b; Manakane, S. et al., 2023). The LULC maps for 2002 and 2023 were utilized to predict the map of 2050 after evaluating the performance of the model.

The percentages of the LULC classes are displayed in Figure 9. The urban areas (UA) and agricultural lands (A) exhibited a considerable increase. The spatial coverage of agricultural lands in 2023 was 2.53%, and increased to 38.93% in 2050. The anticipated urban expansion demands more agricultural land for food supply, which in turn will put considerable pressure on the already-reducing water resources. Consequently, the sustainable planning of the LZRB is essential to conserve its natural resources (Kenea, U. et al., 2021; Leta, M.K. et al., 2021; Gaznayee, H.A.A. et al., 2022).

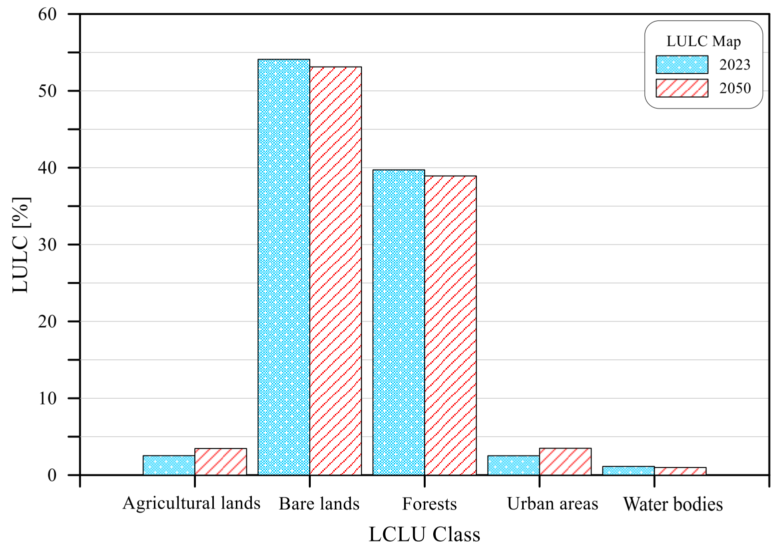

Figure 9: Coverage ratio of LULC in the LZRB in 2023 and 2050

The spatial distribution of LULC within the basin for 2023 and 2050 is shown in Figure 10. The figure clearly shows the decrease in the Dukan reservoir's surface area. Moreover, it can be observed that the agricultural areas expand mainly in the eastern and northeastern parts of the basin.

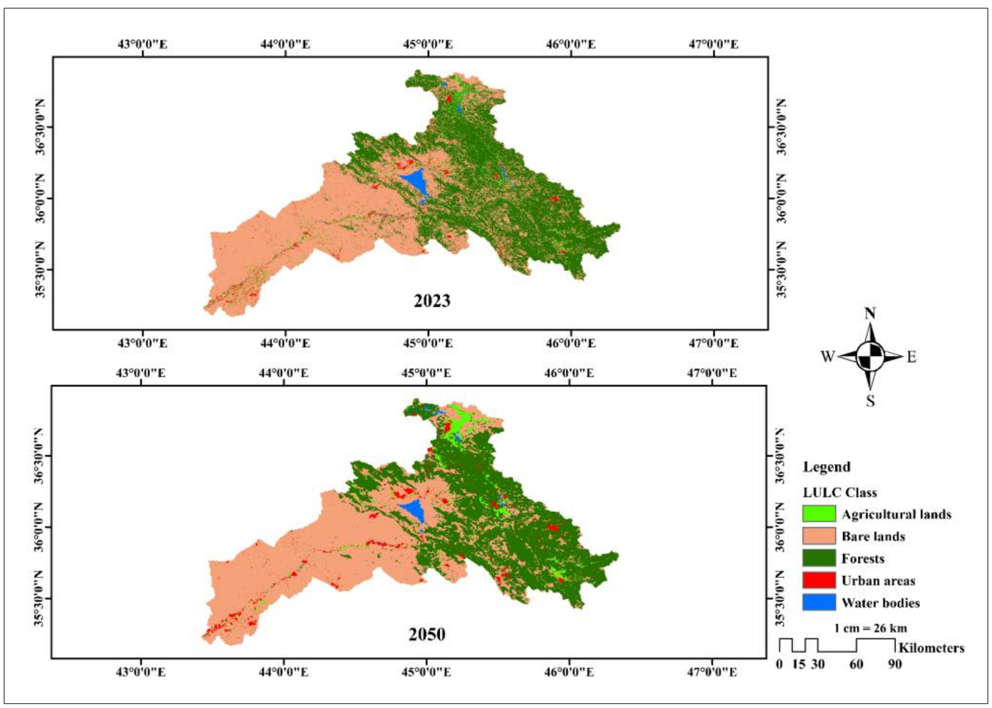

Figure 10: Distribution of LULC within the LZRB in 2023 and 2050

3.5. Future NDVI and LST

A Multiple Linear Regression (MLR) model was applied to determine the future Land Surface Temperature (LST) in the LZRB for the year 2050 (Faqe Ibrahim, G., 2017; Wicki, A. and Parlow, E., 2017).

The regression model obtained using SPSS software, based on 72 points from 2002 and 2013 maps, yielded a coefficient of determination (R^2) of 0.85 for the generated formula. The LST obtained formula is:

$$LST\ (°C) = 331.898 - 0.140 \times Year + 4.496 \times NDVI - 0.007 \times DEM + 1.335 \times BL - 2.054 \times F - 12.182 \times A - 16.924 \times WB - 6.356 \times UA + 3.309 \quad (7)$$

Where:
Year - the required prediction year,
NDVI - the value of Normalized Difference Vegetation Index,
DEM - elevation value,
BL - bare land class,
F - forests class,
A - agricultural lands class,
WB - water bodies class,
UA - urban areas class,
3.309 - standard error of the estimation.

where Year is the required prediction year, NDVI is the value of Normalized Difference, DEM is the elevation value, BL is the bare lands class, F is the forests class, A is the agricultural lands class, WB is the water bodies class, UA is the urban areas class, and 3.309 represents the standard error of the estimation.

After formulating the equation, 36 reference points were selected from the 2023 maps to validate the generated LST formula. The actual and calculated 2023 LST values were plotted, yielding a PBIAS of -8.55 (Very good), R^2 of 0.75 (Good), and NSE of 0.61 (Satisfactory) (Kenea, U. et al., 2021). Moreover, a paired-sample t-test was performed in SPSS; the test accepted the null hypothesis as the significance (2-tailed) was higher than 0.05.

The LULC and NDVI maps in 2050 are required to generate the 2050 LST map. The NDVI maps of 2002 and 2013 were used to project the 2023 map using the CA-Markov model. The resulting K-standard, K-no, and K-location were 0.90, 0.93, and 0.95, respectively. Hence, the 2013 and 2023 NDVI maps were used to project the 2050 map. Figure 11 and Table 7 present the comparison of NDVI classes in 2023 and 2050.

Additionally, Variance Inflation Factor (VIF) and Pearson correlation tests were conducted using the SPSS software to assess the robustness and transparency of the formulated MLR model. All the predictors showed VIF values between 1.05 and 3.65, except for agricultural lands (5.66) and NDVI (8.99), which were also lower than the acceptable limit (≤ 10) (O'brien, M., 2007). The correlation results emphasized the VIF outcomes, as there was no high collinearity between the variables involved. Furthermore, the normal P-P plot indicated that the errors were consistent with the assumption of normal distribution, which in turn enhanced the model's reliability in projecting future LST. Basically, the relatively high VIF values for NDVI and agricultural lands can be attributed to the combined effect of these factors on LST, since pixels classified as agricultural lands exhibited a high NDVI value, similar to pixels classified as forests. However, despite these VIF values, the model precisely estimates LST in the LZRB, as they were lower than 10 (O'brien, M., 2007; Kim, H., 2019).

Table 7: Areas of the NDVI classes in the study area in 2023 and 2050

Year	2023		2050	
Class	Area			
	[km^2]	[%]	[km^2]	[%]
≤ 0	220.1	1.1	210	1.06
0 – 0.2	9201.3	46.5	7643	38.61
0.2 – 0.6	10134.4	51.2	11402	57.60
0.6 – 1	238.2	1.2	541	2.73

The table shows a significant increase in the 0.6–1 class (dense vegetation) from 1.2% in 2023 to 2.73% in 2050. Most of the increment occurred in the northeastern parts (Figure 10). Additionally, the 0.2–0.6 class (sparse vegetation) rose from 51.2% in 2023 to 57.60% in 2050. In contrast, the remaining NDVI classes reduced significantly. The mean NDVI value in 2023 was 0.24, and in 2050, it was 0.33, representing a 37.5% increase from 2023. The increasing NDVI value can be attributed primarily to the growth in agricultural lands and to the decline in both water bodies and bare lands classes.

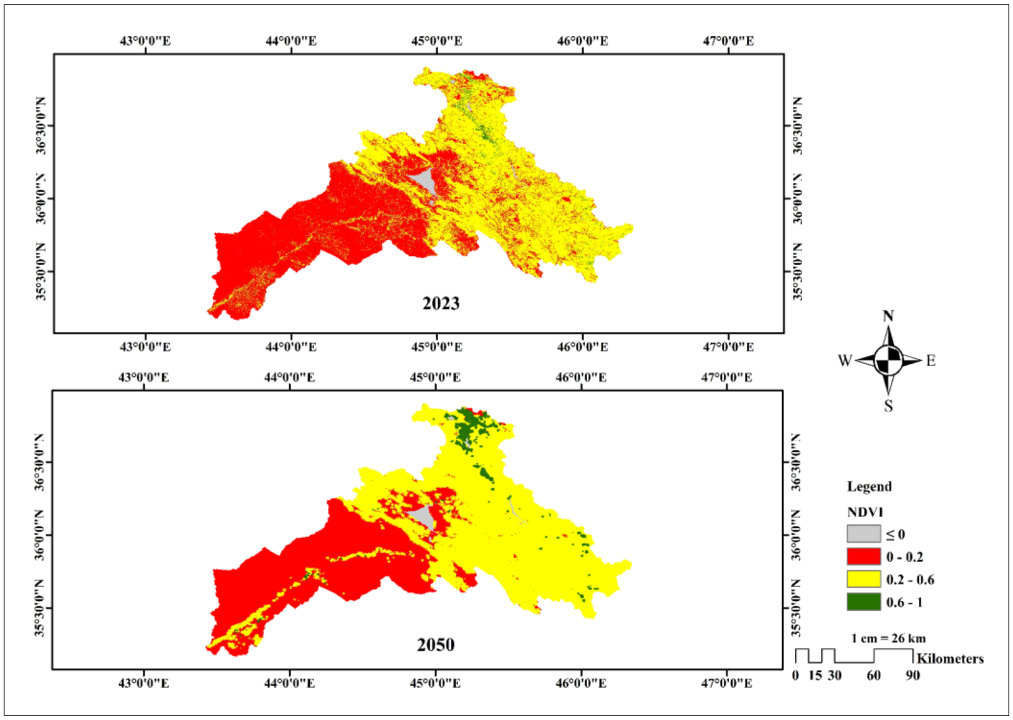

Figure 11: Distribution of NDVI classes within the LZRB in 2023 and 2050

The Raster Calculator in ArcMap was used to determine the LST in 2050 by applying the generated LST formula (Eq. 7). Figure 12 and Table 8 compare the LST classes in 2023 and 2050.

Table 8: Areas of the LST classes within the study area in 2023 and 2050

Year	2023		2050	
Class [°C]	Area			
	[km^2]	[%]	[km^2]	[%]
≤ 30	1236.78	6.25	1595	8.06
30 – 35	2300.63	11.62	4342	21.94
35 – 40	4489.89	22.68	4860	24.55
40 – 45	5495.16	27.76	7596	38.38
45 – 50	5421.87	27.39	1401	7.08
> 50	849.82	4.29	0	0

The spatial extent of all LST classes increased except for the two hottest classes. The class 45–50 °C declined from 5421.87 km^2 in 2023 to 1401 km^2 in 2050, while the class > 50 °C completely vanished. The predominant class in both maps is class 40–45 °C, which covered 27.76% in 2023 and 38.38% in 2050. The mean LST in 2023 and 2050 was 41.29 and 38.14 °C, respectively, with a projected reduction of 7.63%.

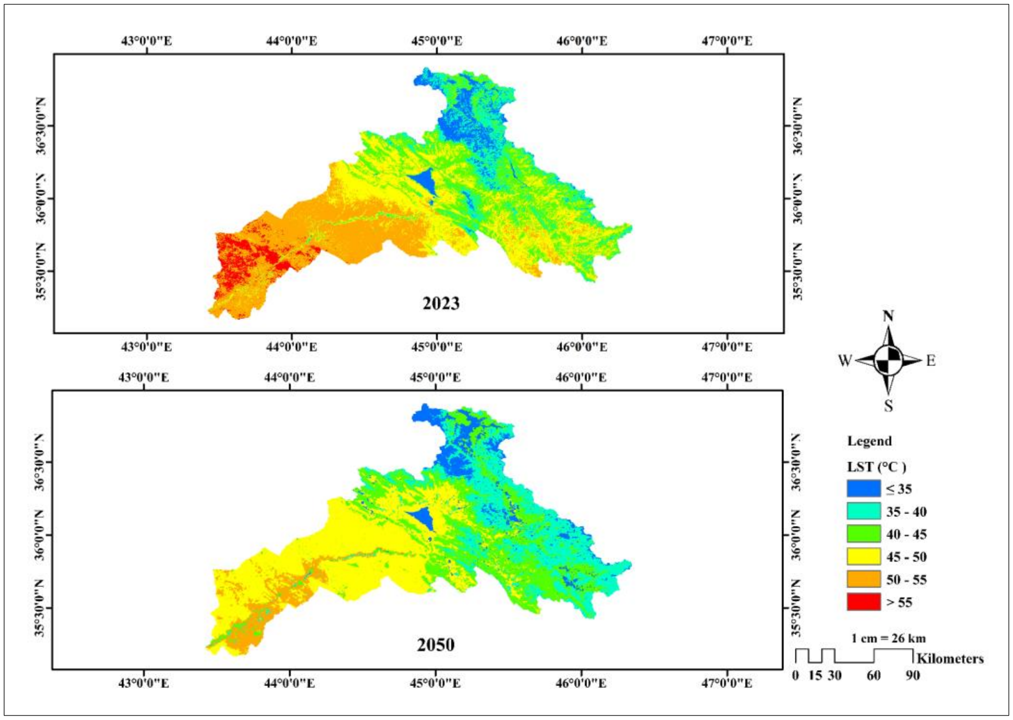

Figure 12: Distribution of LST classes within the LZRB in 2023 and 2050

4. Conclusion

Considerable LULCA occurred in the LZRB due to the population growth and the consequences of climate change. This research aimed to examine LULCA in the basin over the past two decades (2002 to 2023), and to project the LULC pattern in 2050. Furthermore, this study formulated a Multiple Linear Regression (MLR) model to project LST in 2050.

The classification results were almost perfect, with Kappa indices of 0.91, 0.90, and 0.94 for LULC maps in 2002, 2013, and 2023, respectively, and with the lowest overall accuracy of 91.67%. Five LULC classes were identified within the basin: agricultural lands, bare lands, forests, urban areas, and waterbodies. During the baseline period, bare lands and water bodies declined by 8.23% and 13.49%, respectively. In contrast, agricultural lands, forests, and urban areas increased by 42.13%, 7.26%, and 168.09%, respectively.

The mean NDVI value in 2002 was 0.16, increased to 0.20 and 0.24 in 2013 and 2023, respectively. The increasing NDVI value led to a reduction in LST; the mean LST was 44.24 °C in 2002, and declined by 1.80% and 6.67% in 2013 and 2023, respectively.

The CA-Markov model was successfully used to project LULC and NDVI maps for 2050, as the minimum Kappa index (K-standard) was 0.77. The LULC projection results showed an increase in agricultural lands (36.22%) and urban areas (38.49%), while a decline in the remaining LULC classes. The main increase in agricultural lands will take place in the eastern and northeastern parts of the basin. Additionally, the NDVI value increased by 37.50% compared to the 2023 value. Finally, the calibrated regression model yielded a PBIAS, R2, and NSE of -8.55, 0.75, and 0.61, respectively. The projected mean LST over the LZRB declined by 7.63% compared to 2023. Classes 45−50 and > 50 °C were the only shrinking LST classes.

The study projected increased vegetation cover throughout the basin; however, the major driver of this increase is the expansion of agricultural lands. This increment will pose additional stress on the already-reducing surface water resources in the basin. Thus, this study provides stakeholders and planners with thorough insight into past and future environmental conditions to formulate effective and sustainable environmental and water resources strategies within the Little Zab River Basin.

Acknowledgements

The authors would like to thank their institutions. No governmental organizations provided funding for the present research.

Author Contributions

[N. A.] gathered and investigated the data, discussed the outcomes, and wrote and reviewed the manuscript. **[R. M.]** articulated the primary methodology of the study and revised the manuscript.

References

Abbas, N., Wasimia, S., & Al-Ansari, N. (2016). Assessment of climate change impact on water resources of lesser Zab, Kurdistan, Iraq using SWAT model. *Engineering, 8*, 697-715. https://doi.org10.4236/eng.2016.810064

Abburu, S., & Golla, S. B. (2015). Satellite image classification methods and techniques: A review. *International journal of computer applications, 119*(8), 20-25.

Abdulsahib, S., Zubaidi, S., & Ayoob, N. (2024). Using the LARS-WG Model to Predict the Maximum Temperature in Zakho City, Iraq. *Wasit Journal of Engineering Sciences, 12*(4), 214-220. https://doi.org10.31185/ejuow.Vol12.Iss4.563

Ahmed, B., Kamruzzaman, M., Zhu, X., Rahman, M. S., & Choi, K. (2013). Simulating land cover changes and their impacts on land surface temperature in Dhaka, Bangladesh. *Remote Sensing, 5*(11), 5969-5998. https://doi.org10.3390/rs5115969

Al-Doski, J., Mansorl, S. B., & Shafri, H. Z. M. (2013). Image classification in remote sensing. *Journal od Environment and Earth Science, 3*(10).

Al-Saady, Y., Al-Tawash, B., & Al-Suhail, Q. (2016). Effects of land use and land cover on concentrations of heavy metals in surface soils of Lesser Zab River Basin, NE Iraq. *Iraqi Journal of Science, 57*(2C), 1484-1503.

Al-Saady, Y., Al-Tawash, B., Alkinani, M., & Al-Suhail, Q. (2022). Hydrochemical and environmental assessment of groundwaterat the Iraqi part of the Lesser Zab river basin, northeast-Iraq. *Iraqi Bulletin of Geology Mining, 18*(2), 53-74.

Al-sharif, A., & Pradhan, B. (2014). Monitoring and predicting land use change in Tripoli Metropolitan City using an integrated Markov chain and cellular automata models in GIS. *Arabian journal of geosciences, 7*, 4291-4301. https://doi.org10.1007/s12517-013-1119-7

Al-Taei, A., Alesheikh, A., & Darvishi, A. (2023). Land use/land cover change analysis using multi-temporal remote sensing data: A case study of Tigris and Euphrates Rivers Basin. *Land, 12*(5), 1101. https://doi.org10.3390/land12051101

Alex, E., Ramesh, K., & Sridevi, H. (2017). Quantification and understanding the observed changes in land cover patterns in Bangalore. *International Journal of Civil Engineering Technology, 8*(4), 597-603.

Amgoth, A., Rani, P., & Jayakumar, K. (2023). Exploring LULC changes in Pakhal Lake area, Telangana, India using QGIS MOLUSCE plugin. *Spatial Information Research, 31*(4), 429-438. https://doi.org10.1007/s41324-023-00509-1

Atef, I., Ahmed, W., Abdel-Maguid, R., Baraka, M., Darwish, W., & Senousi, A. (2023). Land Use and Land Cover Simulation Based on Integration of Artificial Neural Networks with Cellular Automata-Markov Chain Models Applied to El-Fayoum Governorate. *ISPRS Annals of the Photogrammetry, Remote Sensing Spatial Information Sciences, 10*, 771-777. https://doi.org10.5194/isprs-annals-X-1-W1-2023-771-2023

Ayoob, N., & Mohammed, R. (2025). Possible consequences of land cover and land use dynamics on the land surface temperature: A case study of lower Zab River Basin. *Modeling Earth Systems and Environment, 12*(1). https://doi.org10.1007/s40808-025-02688-2

Chughtai, A., Abbasi, H., & Karas, I. (2021). A review on change detection method and accuracy assessment for land use land cover. *Remote Sensing Applications: Society Environment, 22*, 100482. https://doi.org10.1080/0143116031000101675

Congalton, R. (2001). Accuracy assessment and validation of remotely sensed and other spatial information. *International journal of wildland fire, 10*(4), 321-328. https://doi.org10.1071/WF01031

Costa, R. C. A., Santos, R. M. B., Fernandes, L. F. S., Carvalho de Melo, M., Valera, C. A., Valle Junior, R. F. d., . . . Pissarra, T. C. T. (2023). Hydrologic response to land use and land cover change scenarios: an example from the Paraopeba River basin based on the SWAT model. *Water, 15*(8), 1451. https://doi.org10.3390/w15081451

Das, N., Mondal, P., Sutradhar, S., & Ghosh, R. (2021). Assessment of variation of land use/land cover and its impact on land surface temperature of Asansol subdivision. *The Egyptian Journal of Remote Sensing Space Science, 24*(1), 131-149. https://doi.org10.1016/j.ejrs.2020.05.001

Du, P., Liu, P., Xia, J., Feng, L., Liu, S., Tan, K., & Cheng, L. (2014). Remote Sensing Image Interpretation for Urban Environment Analysis: Methods, System and Examples. *Remote Sensing, 6*(10), 9458-9474. https://doi.org10.3390/rs6109458

Faqe, G. (2017). Urban land use land cover changes and their effect on land surface temperature: Case study using Dohuk City in the Kurdistan Region of Iraq. *Climate, 5*(1), 13. https://doi.org10.3390/cli5010013

Faqe Ibrahim, G. (2017). Urban Land Use Land Cover Changes and Their Effect on Land Surface Temperature: Case Study Using Dohuk City in the Kurdistan Region of Iraq. *Climate, 5*(1). https://doi.org10.3390/cli5010013

Fetene, T., Lohani, K., & Mohammed, K. (2023). LULC change detection using support vector machines and cellular automata-based ANN models in Guna Tana watershed of Abay basin, Ethiopia. *Environmental Monitoring Assessment, 195*(11), 1329. https://doi.org10.1007/s10661-023-11968-2

Gashaw, T., Tulu, T., Argaw, M., & Worqlul, A. (2018). Modeling the hydrological impacts of land use/land cover changes in the Andassa watershed, Blue Nile Basin, Ethiopia. *Science of the Total Environment, 619*, 1394-1408. https://doi.org10.1016/j.scitotenv.2017.11.191

Gaznayee, A., Al-Quraishi, A., Mahdi, K., & Ritsema, C. (2022). A geospatial approach for analysis of drought impacts on vegetation cover and land surface temperature in the Kurdistan Region of Iraq. *Water, 14*(6), 927.

Gaznayee, H. A. A., Al-Quraishi, A. M. F., Mahdi, K., & Ritsema, C. (2022). A geospatial approach for analysis of drought impacts on vegetation cover and land surface temperature in the Kurdistan Region of Iraq. *Water, 14*(6), 927.

Hashim, M., Al-Maliki, A., Sultan, M., Shahid, S., & Yaseen, Z. (2022). Effect of land use land cover changes on land surface temperature during 1984–2020: A case study of Baghdad city using landsat image. *Natural Hazards, 112*(2), 1223-1246. https://doi.org10.1007/s11069-022-05224-y

Idrees, M., Ahmad, S., Khan, M., Dahri, Z., Ahmad, K., Azmat, M., & Rana, I. (2022). Estimation of water balance for anticipated land use in the potohar plateau of the indus basin using SWAT. *Remote Sensing, 14*(21), 5421. https://doi.org10.3390/rs14215421

Jafarzadeh, F., Garakani, A., Maleki, J., Banikheir, M., & Raeesi, R. (2018). *Sealing performance of Silveh embankment dam cutoff wall based on instrumentation measurements*.

Kafy, A., Dey, N., Al Rakib, A., Rahaman, Z., Nasher, R., & Bhatt, A. (2021). Modeling the relationship between land use/land cover and land surface temperature in Dhaka, Bangladesh using CA-ANN algorithm. *Environmental Challenges, 4*, 100190. https://doi.org10.1016/j.envc.2021.100190

Kenea, U., Adeba, D., Regasa, M. S., & Nones, M. (2021). Hydrological responses to land use land cover changes in the Fincha'a Watershed, Ethiopia. *Land, 10*(9), 916. https://doi.org10.3390/land10090916

Khan, M., Tahir, A., Ullah, S., Khan, R., Ahmad, K., Shahid, S., & Nazir, A. (2022). Trends and projections of land use land cover and land surface temperature using an integrated weighted evidence-cellular automata (WE-CA) model. *Environmental Monitoring Assessment, 194*(2), 120. https://doi.org10.1007/s10661-022-09785-0

Kim, H. (2019). Multicollinearity and misleading statistical results. *kja, 72*(6), 558-569. https://doi.org10.4097/kja.19087

Leta, M. K., Demissie, T. A., & Tränckner, J. (2021). Modeling and prediction of land use land cover change dynamics based on land change modeler (Lcm) in nashe watershed, upper blue nile basin, Ethiopia. *13*(7), 3740. https://doi.org10.3390/su13073740

Mahdi, Z., & Mohammed, R. (2022a). Land use/land cover changing aspect implications: Lesser Zab River Basin, northeastern Iraq. *Environmental Monitoring Assessment, 194*(9), 652. https://doi.org10.1007/s10661-022-10324-0

Mahdi, Z., & Mohammed, R. (2022b). *Predicting Land Use/Land Cover Changes in the Lesser Zab River Catchment/Iraq through CA-Markov Synergy Model*.

Manakane, S., Latue, P., Somae, G., & Rakuasa, H. (2023). Prediction of Land Cover Change in Wae Heru Watershed Ambon City Using Celular Automata Markov Chain. *Journal of Geographical Sciences Education, 1*(1), 1-11. https://doi.org10.69606/geography.v1i1.52

Mansourmoghaddam, M., Rousta, I., Cabral, P., Ali, A., Olafsson, H., Zhang, H., & Krzyszczak, J. (2023). Investigation and prediction of the land Use/Land cover (LU/LC) and land surface temperature (LST) changes for Mashhad City in Iran during 1990–2030. *Atmosphere, 14*(4), 741. https://doi.org10.3390/atmos14040741

Masdaf, N., Istijono, B., & Herdianto, R. (2025). Reservoir Capacity Analysis for Flood Mitigation in the Upper Kuranji Watershed. *Civil and Environmental Engineering, 21*(2), 1259-1273. https://doi.org10.2478/cee-2025-0093

Mohammed, R., & Scholz, M. (2024). Climate Change Scenarios for Impact Assessment: Lower Zab River Basin (Iraq and Iran). *Atmosphere, 15*(6), 673. https://doi.org10.3390/atmos15060673

Nath, S., Mishra, G., Kar, J., Chakraborty, S., & Dey, N. (2014). *A survey of image classification methods and techniques*. Paper presented at the 2014 International conference on control, instrumentation, communication and computational technologies (ICCICCT).

O'brien, M. (2007). A Caution Regarding Rules of Thumb for Variance Inflation Factors. *Quality & Quantity, 41*(5), 673-690. https://doi.org10.1007/s11135-006-9018-6

Özturk, B., Uzelli, T., İsbuga, V., & Baba, A. (2023). *Investigation of Hydrological and Hydrogeological Parameters' Alterations in Rapidly Urbanized Regions: Bornova Case (İZmiR, TürkiYe)*.

Pathak, M., Slade, R., Pichs-Madruga, R., Ürge-Vorsatz, D., Shukla, R., & Skea, J. (2022). *Climate Change 2022 Mitigation of Climate Change: Technical Summary*. Retrieved from

Rahem, M., & Mohammed, R. (2025). SWAT-MODFLOW Model for Groundwater Recharge Variation Assessment: Lower Zab River Basin, Northeastern Iraq. *International Journal of Computational and Experimental Science and Engineering*.

Rash, A., Mustafa, Y., & Hamad, R. (2023). Quantitative assessment of Land use/land cover changes in a developing region using machine learning algorithms: A case study in the Kurdistan Region, Iraq. *Heliyon, 9*(11). https://doi.org10.1016/j.heliyon.2023.e21253

Rwanga, S., & Ndambuki, J. (2017). Accuracy assessment of land use/land cover classification using remote sensing and GIS. *International Journal of Geosciences, 8*(04), 611. https://doi.org10.4236/ijg.2017.84033

Sathe, T., & Rahman, S. (2023). Land Use Land Cover Dynamics and its Signature on Land Surface Temperature in Savar, Bangladesh. *Jahangirnagar University Environmental Bulletin, 8*.

Srivastava, P., Han, D., Rico-Ramirez, M., Bray, M., & Islam, T. (2012). Selection of classification techniques for land use/land cover change investigation. *Advances in Space Research, 50*(9), 1250-1265. https://doi.org10.1016/j.asr.2012.06.032

Teshome, D., Leta, M., Taddese, H., Moshe, A., Tolessa, T., Ayele, G., & You, S. (2023). Watershed Hydrological Responses to Land Cover Changes at Muger Watershed, Upper Blue Nile River Basin, Ethiopia. *Water, 15*(14), 2533. https://doi.org10.3390/w15142533

Tran, D., Pla, F., Latorre-Carmona, P., Myint, S., Caetano, M., & Kieu, H. (2017). Characterizing the relationship between land use land cover change and land surface temperature. *ISPRS Journal of Photogrammetry Remote Sensing 124*, 119-132. https://doi.org10.1016/j.isprsjprs.2017.01.001

Ullah, S., Tahir, A., Akbar, T., Hassan, Q., Dewan, A., Khan, A., & Khan, M. (2019). Remote sensing-based quantification of the relationships between land use land cover changes and surface temperature over the Lower Himalayan Region. *Sustainability, 11*(19), 5492. https://doi.org10.3390/su11195492

Voon, K. L., Tan, K. W., & Chin, K. S. (2022). Assessment of the Flood and Drought Occurrence Using Statistically Downscaled Local Climate Models: A Case Study in Langat River Basin, Malaysia. *Civil and Environmental Engineering, 18*(1), 221-233. https://doi.org10.2478/cee-2022-0021

Wicki, A., & Parlow, E. (2017). Multiple Regression Analysis for Unmixing of Surface Temperature Data in an Urban Environment. *Remote Sensing, 9*(7). https://doi.org10.3390/rs9070684

Younus, M., & Mohammed, R. (2023). Geo-informatics techniques for detecting changes in land use and land cover in response to regional weather variation. *Theoretical Applied Climatology, 154*(1), 89-106. https://doi.org10.1007/s00704-023-04536-8

Zadbagher, E., Becek, K., & Berberoglu, S. (2018). Modeling land use/land cover change using remote sensing and geographic information systems: case study of the Seyhan Basin, Turkey. *Environmental Monitoring Assessment, 190*, 1-15. https://doi.org10.1007/s10661-018-6877-y

How to Cite This Article

Ayoob, N., & Mohammed, R. (2026). Land Use and Land Cover and Their Impacts on Land Surface Temperature in the Little Zab River Basin: A Predictive Study. Civil and Environmental Engineering, 0 (0). https://doi.org/10.2478/cee-2026-0083